

**ISTANBUL TECHNICAL UNIVERSITY ★ GRADUATE SCHOOL OF SCIENCE**  
**ENGINEERING AND TECHNOLOGY**

**ICE DETECTION WITH COPLANAR CAPACITIVE SENSOR**



**M.Sc. THESIS**

**Arda AĞAN**

**Department of Mechatronics Engineering**

**Mechatronics Engineering Programme**

**JUNE 2018**



**ISTANBUL TECHNICAL UNIVERSITY ★ GRADUATE SCHOOL OF SCIENCE**  
**ENGINEERING AND TECHNOLOGY**

**ICE DETECTION WITH COPLANAR CAPACITIVE SENSOR**



**M.Sc. THESIS**

**Arda AĞAN**  
**(518131001)**

**Department of Mechatronics Engineering**

**Mechatronics Engineering Programme**

**Thesis Advisor: Assoc. Prof. Dr. Serhat İKİZOĞLU**

**JUNE 2018**



**İSTANBUL TEKNİK ÜNİVERSİTESİ ★ FEN BİLİMLERİ ENSTİTÜSÜ**

**EŞ DÜZLEMLİ KAPASİTİF ALGILAYICI İLE BUZ ALGILAMA**

**YÜKSEK LİSANS TEZİ**

**Arda AĞAN  
(518131001)**

**Mekatronik Mühendisliği Anabilim Dalı**

**Mekatronik Mühendisliği Programı**

**Tez Danışmanı: Doç. Dr. Serhat İKİZOĞLU**

**HAZİRAN 2018**



Arda AĞAN, a M.Sc. student of İTÜ Graduate School of Science Engineering and Technology student ID 518131001, successfully defended the thesis entitled “ICE DETECTING WITH COPLANAR CAPACITIVE SENSOR”, which he prepared after fulfilling the requirements specified in the associated legislations, before the jury whose signatures are below.

**Thesis Advisor :**      **Assoc. Prof. Dr. Serhat İKİZOĞLU** .....  
İstanbul Technical University

**Jury Members :**      **Prof. Dr. Fikret ÇALIŞKAN** .....  
İstanbul Technical University

**Dr. Osman Hilmi KOÇAL** .....  
Yalova University

**Date of Submission : 4 May 2018**  
**Date of Defense : 21 June 2018**







*To my family, to my love*



## **FOREWORD**

First and foremost, my deepest thanks go to my family for providing support to me during the completion of this M.Sc. thesis study. I thank my supervisor Assoc. Prof. Dr. Serhat İKİZOĞLU who has helped me during this thesis and always set the highest of standard for me. Also I am thankful to the my colleagues Hakan TAŞPINAR, M.Sc. Tolga AYTEKİN, Sinem BAŞAR in Development Center Cooling, M.Sc. Emrah ÇETİN and to the management of my company BSH Home Appliances, which has supported to my study.

June 2018

Arda AĞAN  
Mechanical Engineer



## TABLE OF CONTENTS

	<u>Page</u>
<b>FOREWORD</b> .....	<b>ix</b>
<b>TABLE OF CONTENTS</b> .....	<b>xi</b>
<b>ABBREVIATIONS</b> .....	<b>xiii</b>
<b>SYMBOLS</b> .....	<b>xv</b>
<b>LIST OF TABLES</b> .....	<b>xvii</b>
<b>LIST OF FIGURES</b> .....	<b>xix</b>
<b>SUMMARY</b> .....	<b>xxi</b>
<b>ÖZET</b> .....	<b>xxiii</b>
<b>1. INTRODUCTION</b> .....	<b>1</b>
1.1 Objective of the Study.....	1
1.2 Solutions Against the Icing .....	2
1.3 Scope of the Study.....	4
<b>2. SIMULATION OF THE SENSOR</b> .....	<b>7</b>
<b>3. SIGNAL CONDITIONING</b> .....	<b>21</b>
<b>4. SHIELDING</b> .....	<b>25</b>
<b>5. MEASUREMENTS</b> .....	<b>29</b>
<b>6. SENSOR BASED DEFROST ALGORITHM</b> .....	<b>33</b>
<b>7. UNCERTAINTY ANALYSIS</b> .....	<b>35</b>
7.1 Modeling of the Measurement .....	35
7.2 Confidence Interval and Standard Deviation .....	39
<b>8. CONCLUSIONS AND COMMENTS</b> .....	<b>41</b>
<b>REFERENCES</b> .....	<b>43</b>
<b>CURRICULUM VITAE</b> .....	<b>45</b>



## **ABBREVIATIONS**

<b>CCS</b>	: Coplanar Capacitive Sensor
<b>FEA</b>	: Finite Element Analysis
<b>PDEs</b>	: Partial Differential Equations
<b>OP-AMP</b>	: Operational Amplifier
<b>MSO</b>	: Magnetostrictive Oscillator
<b>IR</b>	: Infrared
<b>SBDA</b>	: Sensor Based Defrost Algorithm







## SYMBOLS

<b>C</b>	: Capacitance
<b>V</b>	: Voltage
<b>Q</b>	: Charge
<b><math>\epsilon_r</math></b>	: Dielectric constant of the material between plates
<b><math>\epsilon_0</math></b>	: Permittivity of free space
<b>d</b>	: Distance between the plates
<b><math>\Delta\phi</math></b>	: Differential impedance measurements in potential
<b>r</b>	: Radial distance
<b><math>\theta</math></b>	: Azimuth
<b>z</b>	: Depth
<b><math>\Delta V</math></b>	: The potential difference between the inner and outer annular electrode
<b><math>\epsilon</math></b>	: Permittivity of the medium layer
<b><math>r_{ii}</math></b>	: Inner radial distance of inner electrode
<b><math>r_{io}</math></b>	: Outer radial distance of inner electrode
<b><math>r_{oi}</math></b>	: Inner radial distance of outer electrode
<b><math>r_{oo}</math></b>	: Outer radial distance of outer electrode
<b><math>J_1</math></b>	: 0 <sup>th</sup> order Bessel function of the first kind
<b>t</b>	: Time constant
<b><math>R_A</math></b>	: External resistance which used in signal processing circuit
<b><math>W_r</math></b>	: Uncertainty of the measurement circuit
<b>n</b>	: Independent variable
<b>R</b>	: Dimension will be measured
<b><math>x_n</math></b>	: Variables which effect to measurement
<b><math>w_{x_1}</math></b>	: Error of the independent variables
<b><math>u_c</math></b>	: Combined standard uncertainty
<b><math>u(x)</math></b>	: Standard uncertainty
<b><math>\sigma</math></b>	: Standard deviation



## LIST OF TABLES

	<u>Page</u>
<b>Table 7.1</b> : Ice thickness – sensor capacitance calculations at ANSYS Maxwell....	<b>35</b>
<b>Table 7.2</b> : Uncertainty.....	<b>39</b>





## LIST OF FIGURES

	<u>Page</u>
<b>Figure 1.1</b> : MSO circuit sectional view.....	2
<b>Figure 1.2</b> : Lukas ice detection sensor.....	3
<b>Figure 1.3</b> : Infrared ice detection.....	3
<b>Figure 1.4</b> : Electric fields of parallel plate capacitive sensor.....	4
<b>Figure 2.1</b> : Design 1 simulation 100[mm]*100[mm].....	9
<b>Figure 2.2</b> : Design 2 simulation 100[mm]*100[mm].....	9
<b>Figure 2.3</b> : Design 3 simulation 100[mm]*100[mm].....	9
<b>Figure 2.4</b> : Design 4 simulation 100[mm]*100[mm].....	10
<b>Figure 2.5</b> : Design 5 simulation 100[mm]*100[mm].....	10
<b>Figure 2.6</b> : Design 6 simulation 100[mm]*100[mm].....	10
<b>Figure 2.7</b> : Design 7 simulation 100[mm]*100[mm].....	11
<b>Figure 2.8</b> : Design 8 simulation 100[mm]*100[mm].....	11
<b>Figure 2.9</b> : Design 9 simulation 100[mm]*100[mm].....	11
<b>Figure 2.10</b> :Design 10 simulation 100[mm]*100[mm].....	12
<b>Figure 2.11</b> : Design 11 simulation 100[mm]*100[mm].....	12
<b>Figure 2.12</b> : Design 12 simulation 100[mm]*100[mm].....	12
<b>Figure 2.13</b> : Design 13 simulation 100[mm]*100[mm].....	13
<b>Figure 2.14</b> : Design 14 simulation 100[mm]*100[mm].....	13
<b>Figure 2.15</b> : Design 15 simulation 25[mm]*25[mm].....	13
<b>Figure 2.16</b> : Design 16 simulation 25[mm]*25[mm] with shield.....	14
<b>Figure 2.17</b> : Design 17 simulation 25[mm]*25[mm].....	14
<b>Figure 2.18</b> : Design 18 simulation 25[mm]*25[mm] with acrylic applied.....	15
<b>Figure 2.19</b> : Design 19 simulation 25[mm]*25[mm] with shield.....	15
<b>Figure 2.20</b> : Design 20 simulation 25[mm]*25[mm] with shield lacquer applied..	15
<b>Figure 2.21</b> : Implemented sensor measurement via LCR Meter at 23°C ambient..	16
<b>Figure 2.22</b> : Insulation of the sensor surface via tape at 23°C ambient16	
<b>Figure 2.23</b> : Sensor modeling.....	16
<b>Figure 3.1</b> : Pin configuration of LM555 timer.....	22
<b>Figure 3.2</b> : Monostable waveforms of the LM555 timer.....	22
<b>Figure 3.3</b> : Capacitance – Resistance – Time Delay relation.....	22
<b>Figure 3.4</b> : Signal conditioning circuit at Proteus.....	23
<b>Figure 3.5</b> : Trigger pin signal (pin 2) (blue one) and output pin signal (pin 3) (yellow one) in oscilloscope.....	23
<b>Figure 3.6</b> : Measured capacitance value via software&hardware at 23°C ambient temperature 50% relative humidity.....	24
<b>Figure 4.1</b> : Sensor with shield and w/o shield.....	25
<b>Figure 4.2</b> : The sensor configuration without shield (7,21 [pF]).....	26
<b>Figure 4.3</b> :1[mm] iced and lacquer applied of the without shield sensor surface (10,60 [pF]).....	26
<b>Figure 4.4</b> : The sensor configuration with shield (10,82 [pF]).....	26
<b>Figure 4.5</b> :1[mm] iced and lacquer applied of the with shield sensor surface (13,84 [pF]).....	26

<b>Figure 4.6</b> :Shielded coaxial cable design (inner one is electrode1, middle one is electrode2, outer one is shield).....	27
<b>Figure 4.7</b> :Sensor cable alone capacitance measurement at 23°C ambient temperature 50% relative humidity (12,91[pF]).....	27
<b>Figure 4.8</b> : Shielding of the signal conditioning circuit.....	27
<b>Figure 4.9</b> : Sensor and cable capacitance at 23°C temperature 50% relative humidity 24,79[pF], 12,91[pF] from cable, 11,70[pF] from sensor.....	28
<b>Figure 5.1</b> : Sensor test without icing in the appliance.....	29
<b>Figure 5.2</b> : 40,50[pF] at -30°C temperature 50% relative humidity 16,18[pF] from circuit, 12,91[pF] from cable 11,41[pF] from sensor.....	29
<b>Figure 5.3</b> : Sensor value increases to about 44,67[pF] after door opened.....	29
<b>Figure 5.4</b> : Sensor value about 41,30[pF] after door closed.....	30
<b>Figure 5.5</b> : 1[mm] ice covering to surface of the sensor.....	30
<b>Figure 5.6</b> : Sensor value about 51,69 [pF] after covering with ice as 1[mm] thickness at -30°C temperature 50% relative humidity.....	30
<b>Figure 5.7</b> : Sensor value decreasing to about 46,47[pF] by the time about 10[min].....	31
<b>Figure 5.8</b> : Water drip on the sensor surface.....	31
<b>Figure 5.9</b> : Sensor value 49,72[pF] in case of water drip at -30°C temperature.....	31
<b>Figure 5.10</b> : Sensor value decreasing to about 48,03[pF] by the time about 10[min].....	31
<b>Figure 5.11</b> : Water drip to all of the sensor surface.....	32
<b>Figure 5.12</b> :Sensor value 79,41[pF] in case of water drip to.....	32
<b>Figure 6.1</b> : Sensor Based Defrost Algorithm.....	34
<b>Figure 7.1</b> : Sensor modeling curve.....	36
<b>Figure 7.2</b> : Resistor value 10,02[MΩ] which used in circuit at 25°C temperature.	37
<b>Figure 7.3</b> : Standard deviation graph.....	40

## **ICE DETECTION WITH COPLANAR CAPACITIVE SENSOR**

### **SUMMARY**

Unwanted icing on the cooling appliances is very important in view of cooling performance and energy efficiency. Accumulated ice mass on the freezer decreases the cooling transfer by prevent the air flow contact with cold side of the evaporator. Covering by ice of the coldest zone as called evaporator of the appliance is effect to energy efficiency negatively. A kind of heater is activated for prevent the ice accumulation on the evaporator and it melts the ice by heats the evaporator. In this algorithm as called Defrost, activation of the heater depends on the time, temperature and appliance usage parameters. Activation time and activation duration of the defrost algorithm changes by appliance usage period by user. These durations are calculated by estimation of the algorithm and not be able to detect icing correctly. Therefore, in some cases, even if evaporator zone is not covered by ice, defrost algorithm activates the heater just like evaporator zone is covered by ice and effects the energy efficiency negatively.

In this study, dealed to designing of a sensor which detect the icing. A lot of different coplanar capacitive sensor designs have been designed in simulation tool ANSYS Maxwell Software and ice detection state has been simulated. Fringe effect fields have been used for detecting the icing on the sensor surface. For decreasing the effect of the parasite from environmental factors on sensor and detecting the realistic icing, shield has been applied to rear surface of the sensor. The determined optimum sensor geometry according to ANSYS Maxwell Software results has been realized and measurements have been done with signal conditioning circuit. Protection layered coaxial wire harness has been designed for decrease the parasite effect of the environmental factors to cable which between sensor and signal conditioning circuit.

In signal conditioning circuit, LM555 timer has been used for measuring the sensor charging time and instant capacitance has been determined by time constant instantaneously. An algorithm was created for eliminating the unwanted situations and preventing the misdetection of the icing. Measurement uncertainty analysis has been done according to measurement modeling and considering the uncertainty sourced from components (resistance, timer, etc.) which used in signal conditioning circuit. Besides, each measurement result in signal conditioning circuit has been determined by average of the 30 consecutive measurements.





## EŞ DÜZLEMLİ KAPASİTİF ALGILAYICI İLE BUZ ALGILAMA

### ÖZET

Soğutucu cihazlarda oluşan istenmeyen buzlanma, cihazın soğutma performansı ve verimli çalışması açısından oldukça önemlidir. Dondurucuda biriken buz kütlesi cihazın soğuk kısmı ile hava akışının temasını keserek, ısı transferini azaltır. Cihazın evaporator olarak adlandırılan en soğuk bölgenin buzla kaplanması, enerji verimliliğini olumsuz yönde etkilemektedir. Evaporator bölgesinin buz ile kaplanmasını engellemek için, bir ısıtıcı devreye girerek evaporator bölgesini ısıtır ve buzları eritir. Defrost olarak adlandırılan bu algoritmada, ısıtıcının aktif hale gelmesi zaman, sıcaklık ve cihaz kullanım parametrelerine bağlıdır. Kullanıcının cihazı kullanım sıklığına bağlı olarak, defrost algoritmasının aktifleşme zamanı ve aktif kalma süresi değişmektedir. Bu süreler algoritmanın tahmini olarak hesaplanıp, her buzlanma durumunu doğru olarak tespit edememektedir. Bu sebeple, bazı durumlarda evaporator bölgesi buzlanmadığı halde defrost algoritması, evaporator bölgesi sanki buzluymuş gibi ısıtıcıyı aktifleştirerek enerji tüketimini olumsuz yönde etkilemektedir.

Bu çalışmada, buzlanmayı algılayabilecek bir algılayıcı tasarımı ele alınmıştır. Farklı geometrilerde eş düzlemli kapasitif algılayıcı tasarımları ANSYS Maxwell yazılımı ile simulasyon ortamında tasarlanmış ve buz algılama durumu simüle edilmiştir. Algılayıcının yüzeyinde oluşan buzlanmayı algılamak için saçak etkisi alanları kullanılmıştır. Algılayıcıya çevre etmenlerden gelen gürültünün etkisini azaltmak ve gerçekçi buzlanmayı algılayabilmek için algılayıcının için arka yüzeyine kalkan (shield) uygulanmıştır. ANSYS Maxwell Yazılım'ı sonuçlarına göre belirlenen optimum algılayıcı geometrisi gerçekleştirilip, sinyal koşullama devresi ile ölçüm yapılmıştır. Algılayıcı ile sinyal koşullama devresi arasındaki kablonun, çevre etmenlerden gelen gürültüden etkilenmemesi için çift katmanlı ortak eksenli (coaxial) bir kablo grubu tasarlanmıştır.

Sinyal koşullama devresinde, LM555 zamanlayıcı kullanılarak algılayıcının dolmuş süresi ölçülüp, zaman sabiti ile anlık kapasitans değeri ölçülmüştür. İstenmeyen durumları ortadan kaldırmak ve buzlanmanın yanlış algılanmasını önlemek için bir algoritma oluşturulmuştur. Sinyal koşullama devresinde kullanılan elemanların (direnç, zamanlayıcı vs.) toleranslarından kaynaklanan ölçüm belirsizliği göz önüne alınarak ve ölçüm modellemesine göre, ölçüm belirsizliği analizi yapılmıştır. Ayrıca, sinyal koşullama devresi tarafından yapılan her ölçüm sonucu, ardarda yapılan 30 adet ölçümün ortalaması olarak hesaplanmıştır.



## **1. INTRODUCTION**

Efficiency and performance are the most important issues in the home appliances. Current research and development focus on the less energy consumption and more performance in the home appliances. Same situation is also valid for cooling appliances. Consumer requests low energy consumed high performance, and capable refrigerators. In case of performance and skill ability increased, naturally power consumption is increasing. One of these specifications is No frost. No frost appliances provide the high performance via prevent the icing in the refrigerator. No frost appliances include a function called defrost, and the defrost function includes a heater that operates according to a certain algorithm and timing. The Defrost Function starts with the operation of a heater when the necessary preconditions (time, temperature etc.) are met. During the Defrost, the ambient temperature of the compartment increases for the melting of the ice that accumulates in the appliance. After the Defrost is finished, the compressor starts to cool again.

The Defrost time and duration is calculated as an estimate. It depends on the cooling duration, temperature of the appliance, last Defrost time etc. parameters. The large number of parameters required to determine the defrost time causes the algorithm to become complicated. Moreover, this complex algorithm cannot determine defrosting time precisely. The Defrost that starts at the wrong time causes the heater to operate more than needed even though there is no icing in the environment. This situation leads to an increase in energy consumption.

### **1.1 Objective of the Study**

This study aims to find a method for correctly detect and identify the icing on the parts of the refrigerators that unwanted icing. Thus, precise and timely ice detection can be possible.

This study will present the comparing ice detection states of sensor designs with different geometries and sizes. In this study, the optimal geometry sensor design that

can detect ice is simulated and realized. To obtain a useful signal from the sensor, the signal processor with LM555 timer has been designed and combined with Arduino Uno and Software. This work involves shielding against interference that may affect or distort information coming from the sensor. This work also includes an algorithm for filtering out non-icing conditions detected by the sensor. Also in this study, uncertainty calculations and standard deviations of the measurements made were examined.

**1.2 Solutions Against the Icing**

In most engineering cases, icing is unwanted state in view of performance, efficiency, safety and durability. A lot of kind of different sensor configuration can be used for sensing the icing in different icing problematic cases. For example icing on the aircraft aerodynamic surface is quite critical in view of safety (Aykan, 2005). On the other hand, icing on the wind turbine blades causes the performance decreasing by deration of aerodynamic performance and causes the energy production losses (Froese, 2017). Also, traffic safety can be affected by icing on the highways.

Magnetostrictive sensor is one of the sensor types for ice detection. Magnetostrictive Oscillator (MSO) circuit includes an ultrasonic vibrating probe which vibrates its natural frequency about 40.000 [Hz] (Figure 1.1.). In case of any ice accumulation on the surface of the probe, natural frequency of the probe will be decreased. The electronics circuit calculates the natural frequency of the probe instantaneously. Thus, the thickness of the icing on the probe can be detected (Hoover, 1993).

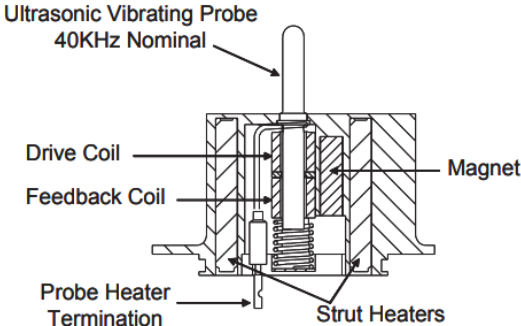


**Figure 1.1 : MSO circuit sectional view.**

Another method is Lukas MK 3 Series ice detector (Figure 1.2). This detector includes a cylinder which driven by a motor and can collect the ice mass. Icing can

be detected by a sharp edge cutter which well nigh to cylinder. In case of icing on the surface of the cylinder, shaving effect will be occurred by the sharp edge cutter. This effect will create an action for the rotating of the motor against a spring. This action affects a micro switch and thus trigger signal can be produced by the micro switch for ice detection (Hoover, 1993).

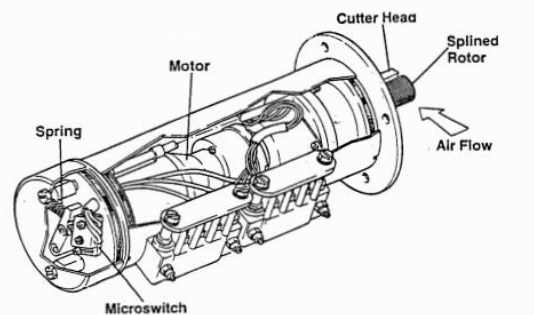


**Figure 1.2 :** Lukas ice detection sensor.

On the other hand, infrared sensors can be used for ice or water detection by examination the reflection of the infrared (IR) source (Figure 1.3). In this method, an emitter and receiver are used and receiver receives the light power from emitter. The power of the emitter moves on the along a reflective material, in common glass, at  $45^\circ$  angles. In case of any ice or water covering the reflective material surface, a part of the power of the emitter take off. When compare the IR rays of the receiver, receiver has weaker IR rays in case of with ice or water covered the reflective material. Thus, ice or water can be detected according to IR ray intensity on the receiver (Semiconductor, 2018).

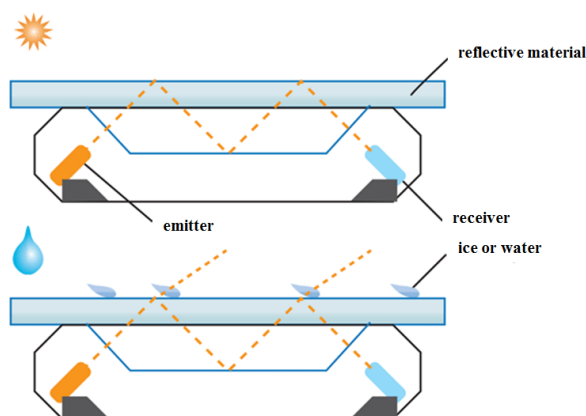


**Figure 1.3 :** Infrared ice detection.

Parallel plate capacitors can be used as a sensor for detecting the icing (Figure 1.4). Parallel plate sensor configuration can be designed basically in small dimensions and needs only two signal cables. With constant space and dielectric constant among of

the plates of sensor the reference capacitance can be calculated. In case of any material which has higher dielectric constant inserted to near of the plates, capacitance value of the sensor changes because of the occurring fringe fields between the plates. Due to ice or water have higher dielectric constant than air, the capacitance value increases (Krebs, 2015).

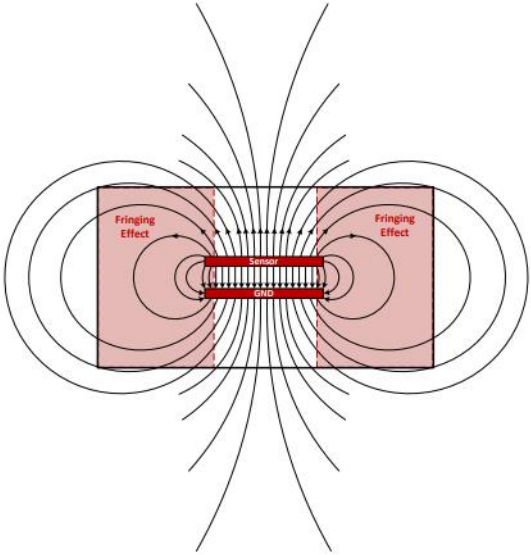


**Figure 1.4 :** Electric fields of parallel plate capacitive sensor.

### 1.3 Scope of the Study

Chapter 2 will explain the basics of the capacitive sensor as physically. Simulation results in ANSYS Maxwell Software will be explained. Simulation results and implemented sensor design results are obtained. A mathematical model of the CCS will be identified.

Chapter 3 will give detailed information about signal processing method for the signal conditioning of the CCS. Basics of the signal conditioning circuit which used in this study will be explained.

Chapter 4 will propose the shielding of the circuit, CCS and wire harness. Designed shielded coaxial cable will be explained. The comparison of the sensor configurations which with shielded to one surface one and without shielded one will be explained.

Chapter 5 will include the measurements by signal conditioning circuit of the sensor which has been inserted to inside of the freezer appliance. Sensor alone, ice and water covered sensor scenarios will be described.

Chapter 6 proposes an algorithm which provide the clear ice detection with consider the another parameters as sensor value, door state of the appliance and ambient temperature.

Chapter 7 includes the uncertainty analysis of the measurements. The measurement modeling and standard deviation calculation will be described.







## 2. SIMULATION OF THE SENSOR

In this study, CCS (coplanar capacitive sensor) has been chosen for detecting the icing. Electrostatic field occurs between charges or potentials in any system of conductors and it calls as capacitance. Basically, capacitance means of electrical charge storing ability of a capacitor (Iossel, 1969). The common form of the capacitance for parallel plate capacitor is shown in equation 1.1. C is the capacitance, Q is the stored charge and V is the voltage.

$$C = \frac{Q}{V} \quad (1.1)$$

As seen in equation 1.2 the definition of the parallel plate capacitor of the two conductors can written as

$$C = \frac{\epsilon_r * \epsilon_0 * A}{d} \quad (1.2)$$

Where A is area of the plates,  $\epsilon_r$  is dielectric constant of the material between plates,  $\epsilon_0$  is permittivity of free space and d is distance between the plates.

Electrostatic field lines orient to lower voltage charged plate from the higher voltage charged one. In addition, fringing effect occurs in edges of the plates. It can be called as also edge effect or fringing field. Besides the calculated capacitance value, fringe effect increases the overall capacitance value of capacitor. In case of any material that has different dielectric constant inserted between the conductor plates of capacitor, capacitance value and fringe effect changes. CCS ensures the wider interaction area in smaller dimensions for capacitance and fringe effect. This is the starting point of the ice detection method via CCS. Dielectric constant of the ice is the three times of the air dielectric constant. Dielectric constant of the water is even greater. In case of any ice or water occurring near of the CCS, capacitance value will be increased. Thus, ice detection will be possible via a sensor.

In this study, ANSYS Maxwell Software has been used for electromagnetic simulations and analysis. ANSYS Maxwell is a Finite Element Analysis (FEA) tool

which use to Maxwell equations for solving the electromagnetic questions. Electromagnetic simulations can be done in a limited finite zone of space by using the suitable boundary conditions [Url-1]. It is fundamental a software which allows the modeling and simulation of a lot of physical fact. Due to the simple user interface and easy modelling, ANSYS Maxwell was chosen to simulate the capacitive sensor and watch the base capacitance before realizing the sensor design.

Firstly, the sensor dimensions chosen as 100[mm]\*100[mm] and simulations have been done in this dimensions. For ease installation and usage of the sensor, sensor has been simulated also in 25[mm]\*25[mm] dimensions. The sensors have been designed and simulated in twenty different configurations. During simulations, the FR4 material thickness has been chosen as 1[mm], copper thickness has been chosen as 0,0347[mm] [Url-2]. The region around the sensor has been chosen as vacuum air and dielectric constant for vacuum air has been chosen as 1, for ice 3. To find the optimum sensor design, the sensor is simulated by applying icing to the sensor surface at specific thickness. Different results obtained in the case of icing, since each sensor design has the same size but has a different interaction area. In the case of increased interaction area, the sensitivity of detecting icing also increases. After the optimum sensor geometry was determined according to the simulation results, the same sensor geometry was simulated with shield. Back surface of the sensor has been shielded with 0,0347[mm] thickness copper and shorted to one of the electrode. In addition, a 0.015[mm] thick acrylic material used on the interaction surface of the sensor to prevent shorting between the electrodes was simulated.

Design 1:

Primitively CCS configuration has been designed with consist of coplanar two plates as capacitor in ANSYS Maxwell Software. In Figure 2.1 length of the electrodes are 100[mm], widths are 20[mm], and distance between electrodes is 60[mm] the potential difference has been applied to coplanar electrodes. The capacitance value has been calculated as 1,11[pF] by software. In case of ice covered the sensor surface with 1[mm] thickness, capacitance value increased to 1,16[pF] by about 4,4% increasing.

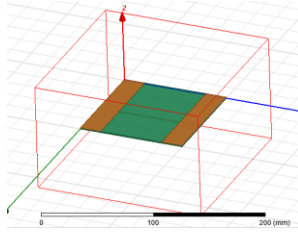


**Figure 2.1 :** Design 1 simulation 100[mm]\*100[mm].

Design 2:

In design 2 shown in Figure 2.2, unlike the initial design, the distance between electrodes decreased to 20[mm] from 60[mm]. The capacitance value has been calculated as 1,78[pF] and when 1[mm] ice applying to sensor surface the capacitance value increased to 1,90[pF] by about 6,7% increasing.

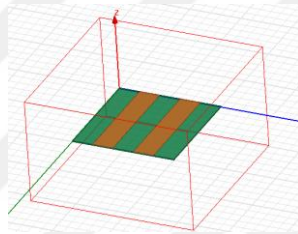


**Figure 2.2 :** Design 2 simulation 100[mm]\*100[mm].

Design 3:

In design 3 shown in Figure 2.3, unlike the initial design, the electrode widths have been increased to 30[mm]. The capacitance value has been calculated as 1,44[pF] and when 1[mm] ice applying to sensor surface the capacitance value increased to 1,51[pF] by about 4,7% increasing.

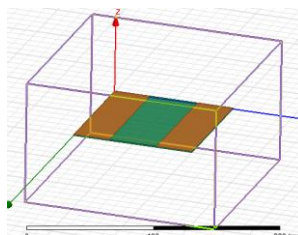


**Figure 2.3 :** Design 3 simulation 100[mm]\*100[mm].

Design 4:

In design 4 shown in Figure 2.4, the electrode widths have been increased to 40[mm]. The capacitance value has been calculated as 1,99[pF] and when 1[mm] ice applying to sensor surface capacitance value increased to 2,12[pF] by about 6,08% increasing.

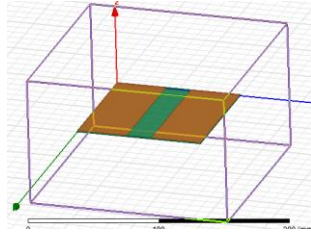


**Figure 2.4 :** Design 4 simulation 100[mm]\*100[mm].

Design 5:

In Figure 2.5, the interaction area has been increased and distance between electrodes has been decreased with “H” shaped design. The capacitance value has been calculated as 7,83[pF] and when 1[mm] ice applying to sensor surface capacitance value increased to 9,26[pF] by about 18,16% increasing.

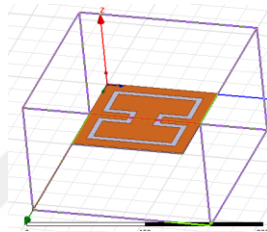


**Figure 2.5 :** Design 5 simulation 100[mm]\*100[mm].

Design 6:

The dimensions of the electrodes have been changed in Figure 2.6. The capacitance value has been calculated as 7,67[pF] and when 1[mm] ice applying to sensor surface capacitance value increased to 9,02[pF] by about 17,53% increasing. In design 6, according to design 5, the result is not very different.

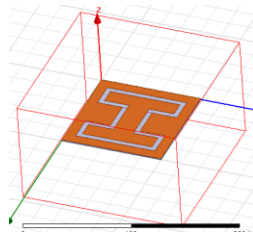


**Figure 2.6 :** Design 6 simulation 100[mm]\*100[mm].

Design 7:

Comb shaped electrodes has been designed in Figure 2.7. The capacitance value has been calculated as 8,66[pF] and when 1[mm] ice applying to sensor surface capacitance value increased to 10,32[pF] by about 19,22% increasing. This result is better than the primitively ones and “H” shaped ones.

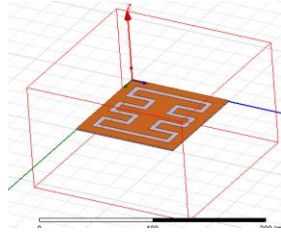


**Figure 2.7 :** Design 7 simulation 100[mm]\*100[mm].

Design 8:

Middle part of the comb design has been thinned to 10[mm] in Figure 2.8 from 20[mm]. The capacitance value has been calculated as 9,17[pF] and when 1[mm] ice applying to sensor surface capacitance value increased to 11,0[pF] by about 20% increasing.

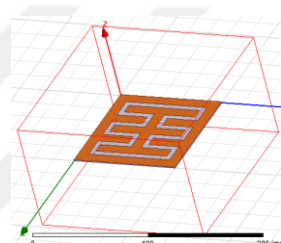


**Figure 2.8 :** Design 8 simulation 100[mm]\*100[mm].

Design 9:

The comb design has been cancelled in one of the electrodes to see the effect of it in Figure 2.9. The capacitance value has been calculated as 6,01[pF] and when 1[mm] ice applying to sensor surface capacitance value increased to 7,0[pF] by about 16,37% increasing. This shows that capacitance change decreases because of the electrode area decreasing.

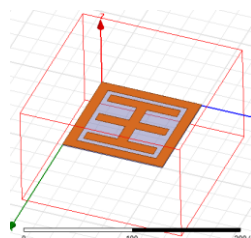


**Figure 2.9 :** Design 9 simulation 100[mm]\*100[mm].

Design 10:

In Figure 2.10 “S” shaped interaction area has been designed. The capacitance value has been calculated as 4,95[pF] and when 1[mm] ice applying to sensor surface capacitance value increased to 5,68[pF] by about 14,79% increasing.

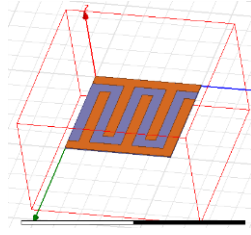


**Figure 2.10** : Design 10 simulation 100[mm]\*100[mm].

Design 11:

In design 11 as shown in Figure 2.11, unlike the design 10, electrodes have been designed as corrugated shape for increasing the electrode area and interaction area. The capacitance value has been calculated as 5,83[pF] and when 1[mm] ice applying to sensor surface capacitance value increased to 6,83[pF] by about 17,04% increasing.

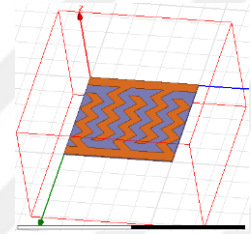


**Figure 2.11** : Design 11 simulation 100[mm]\*100[mm].

Design 12:

In Figure 2.12 the distance between electrodes decreased to 5[mm] from 10[mm] which in design 10. Thus, total electrode area also increased due to more close electrodes. The capacitance value has been calculated as 8,68[pF] and when 1[mm] ice applying to sensor surface capacitance value increased to 10,27[pF] by about 18,33% increasing.

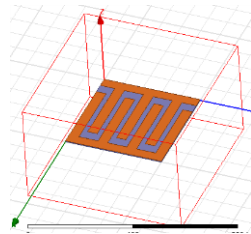


**Figure 2.12** : Design 12 simulation 100[mm]\*100[mm].

Design 13:

In design 13 as shown in Figure 2.13, unlike the before design 12, electrodes have been designed as corrugated shape. The capacitance value of the sensor has been

calculated as 9,65[pF] and when 1[mm] ice applying to sensor interaction surface, the capacitance value has been increased to value 11,81[pF] by about 22,31% increasing ratio.

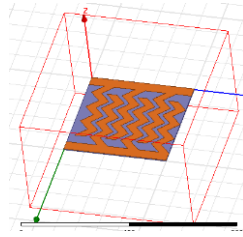


**Figure 2.13 :** Design 13 simulation 100[mm]\*100[mm].

Design 14:

Circular electrodes has been designed in Figure 2.14 for ensure the maximum electrode area and interaction area. The capacitance value has been calculated as 18,69[pF] and when 1[mm] ice applying to sensor surface capacitance value increased to 24,08[pF] by about 28,83% increasing. This increasing ratio is the best result in the simulation results in different geometries.

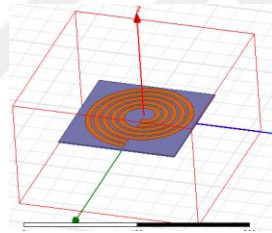


**Figure 2.14 :** Design 14 simulation 100[mm]\*100[mm].

Design 15:

In Figure 2.15 design 15 is the re-design of the design 1 with shield application and dimension decreasing to 25[mm]\*25[mm] from 100[mm]\*100[mm]. The capacitance value has been calculated as 0,42[pF] and when 1[mm] ice applying to sensor surface capacitance value increased to 0,47[pF] by about 12% increasing.

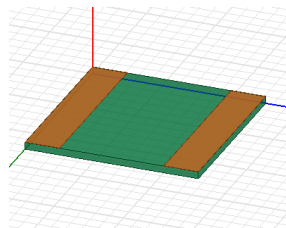


**Figure 2.15 :** Design 15 simulation 25[mm]\*25[mm].

Design 16:

In Figure 2.16 design 16 is the re-design of the design 15 with shield application and dimension decreasing to 25[mm]\*25[mm] from 100[mm]\*100[mm]. The capacitance value has been calculated as 5,9[pF] and when 1[mm] ice applying to sensor surface capacitance value increased to 6,1[pF] by about 4,6% increasing.

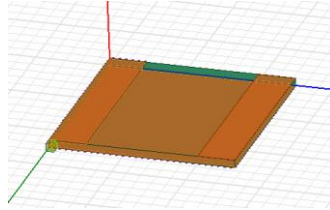


**Figure 2.16 :** Design 16 simulation 25[mm]\*25[mm] with shield.

Design 17:

In Figure 2.17 design 17 is the re-design of the design 14 with dimension decreasing to 25[mm]\*25[mm] from 100[mm]\*100[mm]. The capacitance value has been calculated as 7,2[pF] and when 1[mm] ice applying to sensor surface capacitance value increased to 10,1[pF] by about 41% increasing.

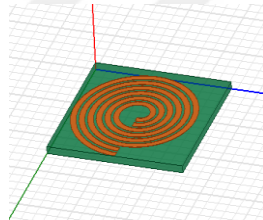


**Figure 2.17 :** Design 17 simulation 25[mm]\*25[mm].

Design 18:

In design 18 in Figure 2.18, the acrylic material has been covered the interaction surface of the sensor. The capacitance value has been calculated as 7,7[pF] and when 1[mm] ice applying to sensor surface capacitance value increased to 10,6[pF] by about 36% increasing. This result shows that, acrylic material covering does not effect extremely the sensor capacitance value without ice covering but effects to icing sensitivity negatively in case of ice covering.



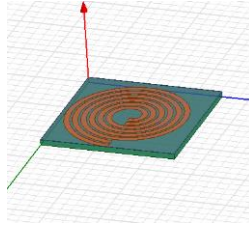


**Figure 2.18 :** Design 18 simulation 25[mm]\*25[mm] with acrylic applied.

Design 19:

In Figure 2.19 shows that, shield applied to design 17. The capacitance value has been calculated as 10,82[pF] and when 1[mm] ice applying to sensor surface capacitance value increased to 13,4[pF] by about 24% increasing. This result shows shielding of the one side of the sensor effects the icing sensitivity negatively.

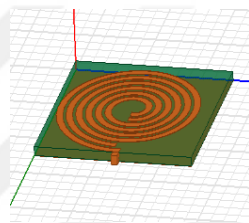


**Figure 2.19 :** Design 19 simulation 25[mm]\*25[mm] with shield.

Design 20:

In Figure 2.20, design 20 consists of together shielding and acrylic material covering. The capacitance value has been calculated as 11,3[pF] and when 1[mm] ice applying to sensor surface capacitance value increased to 13,8[pF] by about 22% increasing.

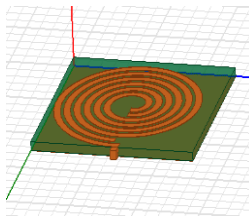


**Figure 2.20 :** Design 20 simulation 25[mm]\*25[mm] with shield lacquer applied.

According to simulation results, the design 20 has been implemented. In Figure 2.21, the implemented sensor geometry has been measured via a LCR Meter for the comparison with ANSYS Maxwell results. The value is about 11,51[pF] in LCR meter and about 10,82[pF] in ANSYS Maxwell Software. For prevent the short cut of the electrodes on the sensor surface, sensor surface has been insulated by a thin acrylic tape. This situation has been also implemented and simulated. In Figure 2.22

the implemented tape applied sensor value with LCR Meter is about 11,70[pF] and ANSYS Maxwell result for the tape applied sensor configuration about 11,32[pF]. In Maxwell simulation, tape material has been selected as acrylic with 0,015[mm] thickness and with 3,6 dielectric constant [Url-3].



**Figure 2.21** : Implemented sensor measurement via LCR Meter at 23°C ambient temperature 50% relative humidity (11,51 pF).



**Figure 2.22** : Insulation of the sensor surface via tape at 23°C ambient temperature 50% relative humidity (11,70 pF).

Sensor modeling in Figure 2.23 the origin of a cylindrical-coordinate system is on the middle of the electrodes.

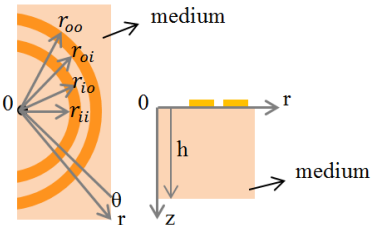


**Figure 2.23** : Sensor modeling.

The Laplace equation is defined as in equation 2.1.

$$\Delta\varphi = \frac{1}{r} + \frac{\partial}{\partial r} \left( r \frac{\partial\varphi}{\partial r} \right) + \frac{1}{r^2} \frac{\partial^2\varphi}{\partial\theta^2} + \frac{\partial^2\varphi}{\partial z^2} = 0 \quad (2.1)$$

where  $r$  is the radial distance,  $\theta$  is the azimuth, and  $z$  is the depth. Azimuth  $\theta$  is not a factor of electric potential  $\varphi$  in the medium cause of the electrodes are swept throughout environmental direction, can be rewritten as shown in equation 2.2.

$$\Delta\varphi = \frac{\partial^2\varphi}{\partial r^2} + \frac{1}{r} \frac{\partial\varphi}{\partial r} + \frac{\partial^2\varphi}{\partial z^2} = 0 \quad (2.2)$$

The boundary conditions of the Laplace equation produce the below result:

(A)  $\Delta V$  is defined as the potential difference between the inner and outer annular electrode on the interface between electrodes and medium as defined in equation 2.3.

$$\varphi|_{z=0, r_{ii} < r < r_{io}} - \varphi|_{z=0, r_{oi} < r < r_{oo}} = \Delta V \quad (2.3)$$

(B) In other fields of the same interface, the z-direction of the electric field density is zero as below equation 2.4.

$$\frac{\partial\varphi}{\partial z} \Big|_{z=0, 0 < r < r_{ii}} = \frac{\partial\varphi}{\partial z} \Big|_{z=0, r_{io} < r < r_{oi}} = \frac{\partial\varphi}{\partial z} \Big|_{z=0, r_{oo} < r < r_{\infty}} = 0 \quad (2.4)$$

(C) On the bottom surface of the medium, the z-direction of the electric field density is zero as described in equation 2.5.

$$\frac{\partial\varphi}{\partial z} \Big|_{z=h} = 0 \quad (2.5)$$

(D) With region integration of the electric density, the rough equations of the electric amount on the inner and the outer annular electrodes can be defined as in equation 2.6 and equation 2.7.

$$Q \approx \int_0^{\theta_0} \int_{r_{ii}}^{r_{io}} \epsilon \left( -\frac{\partial\varphi}{\partial z} \Big|_{z=0} \right) r dr d\theta \approx \epsilon + \frac{r_{io}^2 - r_{ii}^2}{2} \theta_0 \left( -\frac{\partial\varphi}{\partial z} \Big|_{z=0, r_{ii} < r < r_{io}} \right) \quad (2.6)$$

$$-Q \approx \int_0^{\theta_0} \int_{r_{oi}}^{r_{\infty}} \epsilon \left( -\frac{\partial \varphi}{\partial z} \Big|_{z=0} \right) r dr d\theta \approx \epsilon + \frac{r_{\infty}^2 - r_{oi}^2}{2} \theta_0 \left( -\frac{\partial \varphi}{\partial z} \Big|_{z=0, r_{oi} < r < r_{\infty}} \right) \quad (2.7)$$

Then, there are another two conditions as shown in equation 2.8 and equation 2.9.

$$-\frac{\partial \varphi}{\partial z} \Big|_{z=0, r_{ii} < r < r_{io}} \approx \frac{2Q}{\epsilon(r_{io}^2 - r_{ii}^2)} \theta_0 \quad (2.8)$$

$$-\frac{\partial \varphi}{\partial z} \Big|_{z=0, r_{oi} < r < r_{\infty}} \approx \frac{2Q}{\epsilon(r_{\infty}^2 - r_{oi}^2)} \theta_0 \quad (2.9)$$

For solving of the Laplace equation, a zeroth-order Hankel transform is used, equation 2.2 is defined as in equation 2.10.

$$\frac{\partial^2 \Psi(\zeta, z)}{\partial z^2} - \zeta^2 \Psi(\zeta, z) = 0 \quad (2.10)$$

A general solution can be written as shown in equation 2.11.

$$\Psi(\zeta, z) = K_1 e^{-\zeta z} + K_2 e^{\zeta z} \quad (2.11)$$

For boundary condition C in equation 2.12.

$$\frac{\partial \Psi(\zeta, z)}{\partial z} \Big|_{z=h} = 0 \quad (2.12)$$

For boundary conditions B and D in equation 2.13.

$$-\frac{\partial \Psi(\zeta, z)}{\partial z} \Big|_{z=0} = \frac{2Q}{\epsilon \theta_0} \left[ \frac{r_{io} J_1(\zeta r_{io}) - r_{ii} J_1(\zeta r_{ii})}{\zeta(r_{io}^2 - r_{ii}^2)} - \frac{r_{\infty} J_1(\zeta r_{\infty}) - r_{oi} J_1(\zeta r_{oi})}{\zeta(r_{\infty}^2 - r_{oi}^2)} \right] \quad (2.13)$$

With solution of the equation 2.11 using converted boundary equations 2.12 and 2.13, there is a particular solution for equation 2.10 as shown in equation 2.14.

$$\partial \Psi(\zeta, z) = \frac{2Q}{\epsilon \theta_0} \frac{\cosh[\zeta(h-z)]}{\zeta \sinh(\zeta h)} \left[ \frac{r_{io} J_1(\zeta r_{io}) - r_{ii} J_1(\zeta r_{ii})}{\zeta(r_{io}^2 - r_{ii}^2)} - \frac{r_{\infty} J_1(\zeta r_{\infty}) - r_{oi} J_1(\zeta r_{oi})}{\zeta(r_{\infty}^2 - r_{oi}^2)} \right] \quad (2.14)$$

For this reason, the inverse zeroth-order Hankel transform of equation 2.14 aids to solving of the first Laplace equation as below equation 2.15.

$$\varphi(r, z) = \int_0^{\infty} \Psi(\zeta, z) J_0(\zeta r) \zeta d\zeta \quad (2.15)$$

The mean value used over the surface integration as an approach of the electrode electric potential, as described in equation 2.16 and equation 2.17.

$$\varphi|_{z=0, r_{ii} < r < r_{io}} = \frac{\theta_0 \int_{r_{ii}}^{r_{io}} \varphi(r, z)|_{z=0} r dr}{\frac{\theta_0}{2} (r_{io}^2 - r_{ii}^2)} \quad (2.16)$$

$$\varphi|_{z=0, r_{oi} < r < r_{\infty}} = \frac{\theta_0 \int_{r_{oi}}^{r_{\infty}} \varphi(r, z)|_{z=0} r dr}{\frac{\theta_0}{2} (r_{\infty}^2 - r_{oi}^2)} \quad (2.17)$$

With integration of the boundary condition in A in equation 2.3, equation 2.18 can be written as below.

$$\Delta V = \frac{4Q}{\epsilon\theta_0} \int_0^{\infty} \frac{\left[ \frac{r_{io} J_1(\zeta r_{io}) - r_{ii} J_1(\zeta r_{ii})}{\zeta (r_{io}^2 - r_{ii}^2)} - \frac{r_{\infty} J_1(\zeta r_{\infty}) - r_{oi} J_1(\zeta r_{oi})}{\zeta (r_{\infty}^2 - r_{oi}^2)} \right]^2}{\tan h(\zeta h)} d\zeta \quad (2.18)$$

According to definitions, a mathematical definition of capacitance value C can be written as (Guo, Hu, and Tan, 2016) as below equation 2.19.

$$C = \frac{Q}{\Delta V} \quad (2.19)$$

$$= \epsilon\theta_0 \frac{1}{4 \int_0^{\infty} \frac{\left[ \frac{r_{io} J_1(\zeta r_{io}) - r_{ii} J_1(\zeta r_{ii})}{\zeta (r_{io}^2 - r_{ii}^2)} - \frac{r_{\infty} J_1(\zeta r_{\infty}) - r_{oi} J_1(\zeta r_{oi})}{\zeta (r_{\infty}^2 - r_{oi}^2)} \right]^2}{\tan h(\zeta h)} d\zeta}$$

The analytical model in Equation (2.19), capacitance value C is calculated by a Finite Element Analysis (FEA). The electrostatic field analysis based on a finite element method is possible with ANSYS Maxwell Software.



### 3. SIGNAL CONDITIONING

For process the output signal of any sensor, signal conditioning circuits are used. In this study, the circuit with LM555 timer has been designed for signal processing of the CCS output. LM555 timer in Figure 3.1 includes an operational amplifier (OP-AMP) which operates as comparator. A comparator is basic device which provides the comparison of the voltages at the inputs. In monostable working mode of LM555 timer, the CCP is initially keeping discharged by a transistor within timer. In case of a negative trigger pulse applying of less than  $1/3$  VCC to pin 2, the flip-flop toggles the output as high. The voltage against the capacitor increases exponentially during the period of  $t$  as shown in equation 3.1, until the voltage equals  $2/3$  VCC. Figure 3.2 shows the wave shapes occurring in this monostable working mode. The waveform on the top is trigger pin (pin 2), middle one is the output pin (pin 3) and below one is the threshold pin (pin 6). The output will then remain in the low state until a trigger pulse is again applied [Url-4]. A push button switch has been used for initialising the trigger pulse applying. One input pin of the Arduino UNO detects the pushed the switch the toggle the trigger pin (pin 2) LOW from HIGH. Thus output pin (pin 3) toggled to HIGH from LOW till CCS charged to  $2/3$  VCC. Toggle of the output pin (pin 3) can be detected by Arduino attachInterrupt function [Url-5]. Instant capacitance value of the CCS is calculated according to equation 3.1. This process repeats 30 times per measurement and average value of 30 measurement results is calculating as result.  $t$  is the duration of the CCS charged to  $2/3$  VCC from 0 VCC,  $R_A$  is the external resistance which used in signal processing circuit and  $C$  is the capacitance value which will be measured.

$$t = 1.1 * R_A * C \quad (3.1)$$

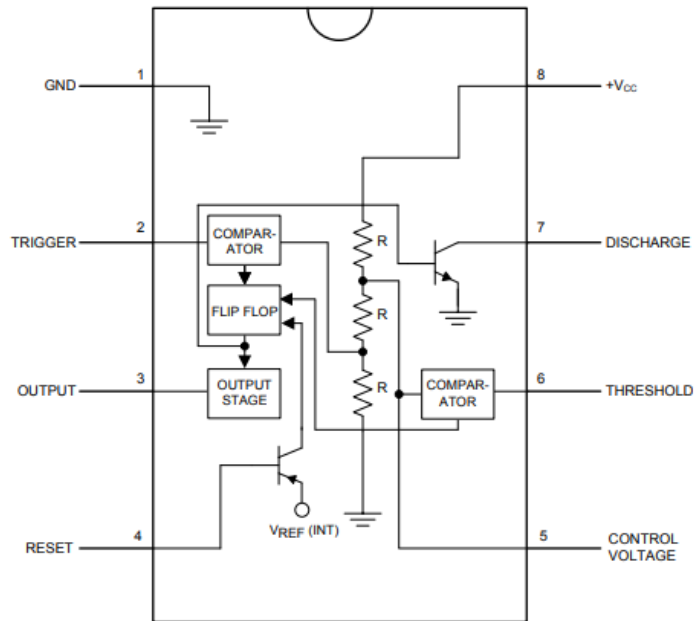


**Figure 3.1 :** Pin configuration of LM555 timer.

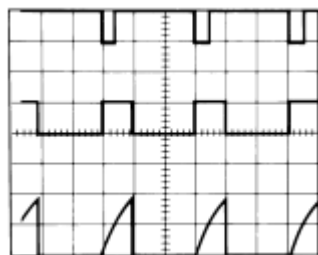


**Figure 3.2 :** Monostable waveforms of the LM555 timer.

Defining of the external resistance  $R_A$  is done according to curve of the capacitance-resistance-time delay as  $10 \text{ M}\Omega$  shown in Figure 3.3.

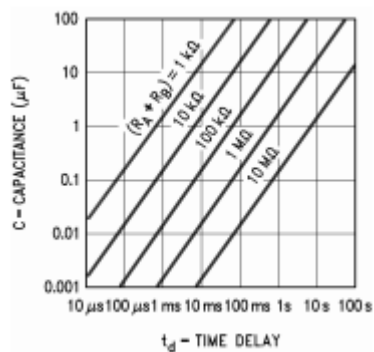


**Figure 3.3 :** Capacitance – Resistance – Time Delay relation.

Also, circuit modeled in Proteus Software in Figure 3.4. The circuit without connected sensor has been tested via oscilloscope in Figure 3.5.



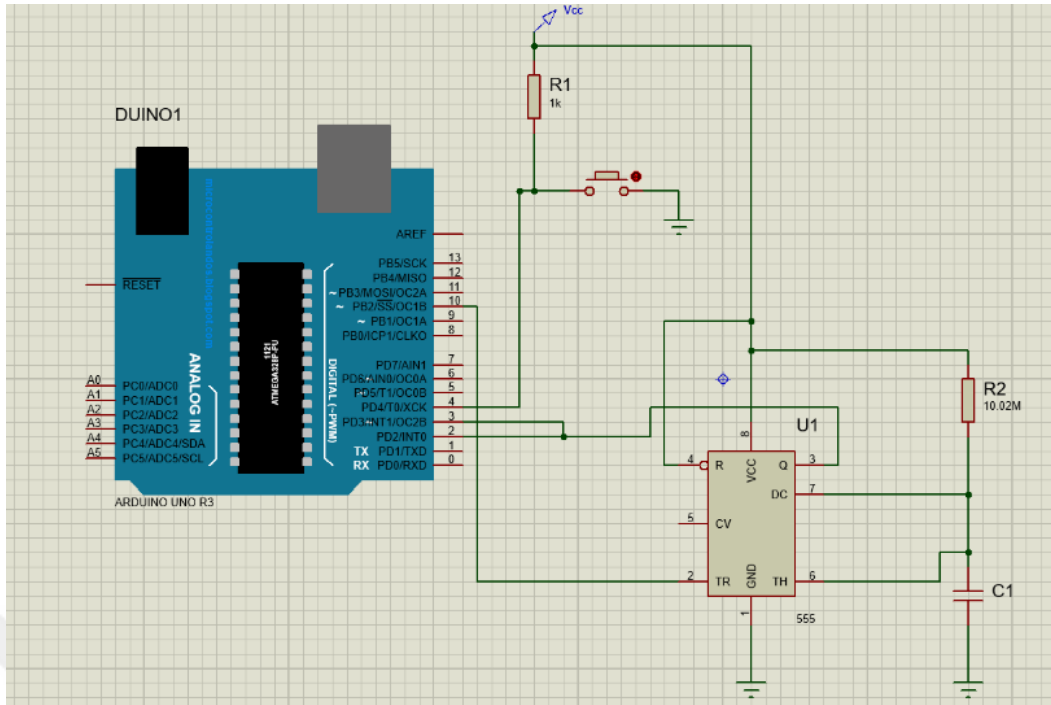


**Figure 3.4 :** Signal conditioning circuit at Proteus.

One port of the oscilloscope has been connected to trigger pin of the LM555 timer and another one has been connected to output pin of the LM555 timer. In Figure 3.5 the duration from beginning time of the trigger detection till the duration which measured for charging till  $2/3$  VCC the internal capacitance of the circuit is about  $180 \mu\text{s}$ . The capacitance value for this duration about  $16[\text{pF}]$  in Figure 3.6. This value also calculated in equation 3.2 and equation 3.3.

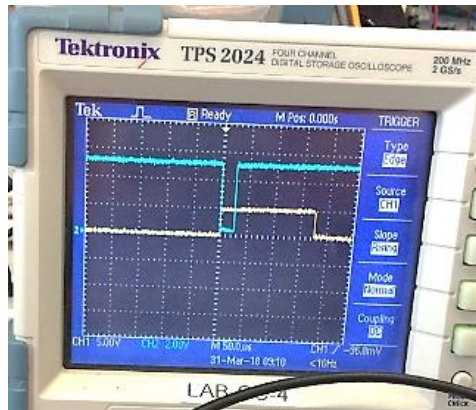


**Figure 3.5 :** Trigger pin signal (pin 2) (blue one) and output pin signal (pin 3) (yellow one) in oscilloscope.

```

t = 180microseg
C = 0,00 nanoF
C = 16,36 pikof
C = 16363,64 femtoF
C = 16363645,00 attoF
16000,00 ;16363,64 ;
ave;16,18pikof

```

**Figure 3.6 :** Measured capacitance value via software&hardware at 23°C ambient temperature 50% relative humidity.

$$180 * 10^{-6} = 1.1 * 10 * 10^6 * C \quad (3.2)$$

$$C = \frac{180 ** 10^{-6}}{1.1 * 10 * 10^6} \cong 16[pF] \quad (3.3)$$

#### 4. SHIELDING

Sensor working principle is based on capacitive and fringe effect which quite weak and responsive to environmental parasites. Some environmental parasites in the neighborhood of the sensor such as any component which diffuse parasites activation or water drip can effect the accuracy of the sensor. For decreasing the parasite effect to sensor surface, one side of the sensor has been shielded in Figure 4.1. In case of any voltage apply to CH electrode while the GND is a fixed ground reference, there are electrostatic field lines (red ones) from the higher voltage potential (CH) to lower voltage potential electrode (GND). When there is no any shield electrostatic field lines are orient above and below the sensor plane symmetrically and sensor can detect the ice above and the below. When there is a shield under side of the sensor as CH and GND electrodes, the electrostatic field lines will occur in only one side of the sensor and precision of the sensor will be decreased (Wang, 2015).

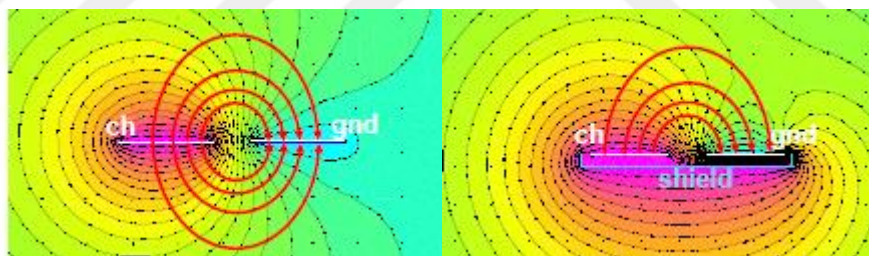


**Figure 4.1 :** Sensor with shield and w/o shield.

The sensor configurations with shield and without shield have been simulated in ANSYS Maxwell Software. In Figure 4.2 the capacitance value 7,2[pF] for without shield sensor configuration increased to 10,1[pF] by 1[mm] ice thickness in Figure 4.3 as 41% increasing ratio. On the other hand, in Figure 4.4 the capacitance value 10,82[pF] for with shield sensor configuration increased to 13,84[pF] by 1[mm] ice thickness in Figure 4.5 as 22% increasing ratio.

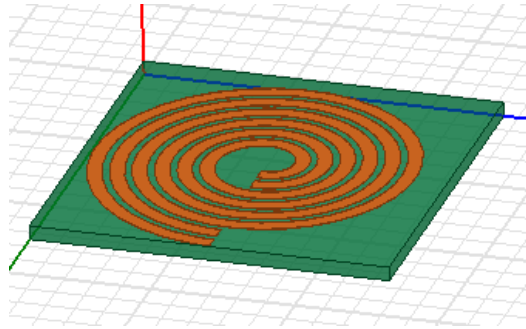


**Figure 4.2 :** The sensor configuration without shield (7,21 [pF]).

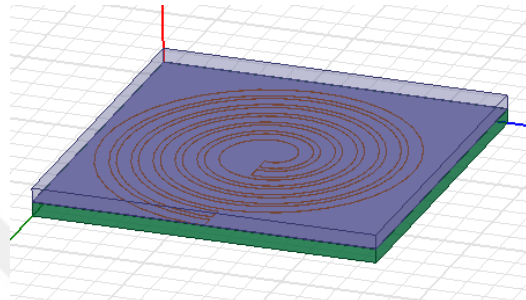


**Figure 4.3 :** 1[mm] iced and lacquer applied of the without shield sensor surface (10,60 [pF]).

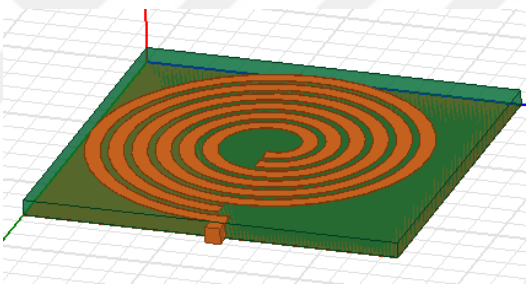


**Figure 4.4 :** The sensor configuration with shield (10,82 [pF]).

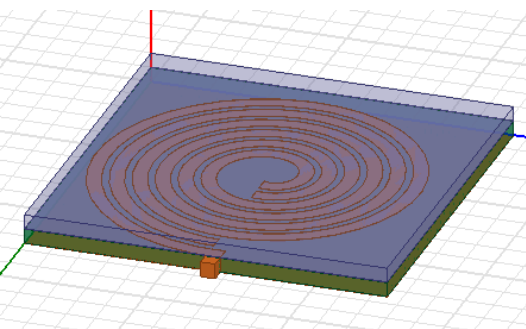


**Figure 4.5 :** 1[mm] iced and lacquer applied of the with shield sensor surface (13,84 [pF]).

Besides, parasites can affect the wire harness between CCS and signal conditioning circuit. Cables can pick up the parasites along the line. In Figure 4.6 a coaxial cable which provides shielding from environmental parasites has been designed. In addition, the cable length between sensor and signal conditioning has been designed

as short as possible. Thus internal capacitance of the cable also has been decreased. The internal capacitance of the cable alone has been measured with LCR meter in Figure 4.7.



**Figure 4.6 :** Shielded coaxial cable design (inner one is electrode1, middle one is electrode2, outer one is shield).

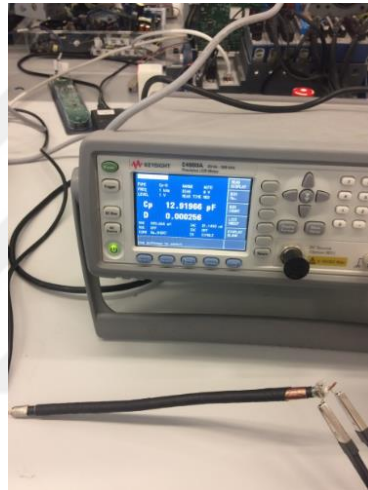


**Figure 4.7 :** Sensor cable alone capacitance measurement at 23°C ambient temperature 50% relative humidity (12,91[pF]).

Also signal conditioning circuit can be subject of environmental parasites. So all surfaces of the signal conditioning circuit has been shielded by covering the aluminum cover as below in Figure 4.8.

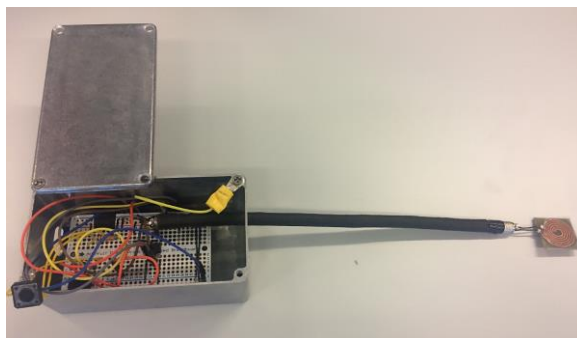


**Figure 4.8 :** Shielding of the signal conditioning circuit.

The sensor has been soldered to shielded coaxial cable and the total capacitance of the sensor and the cable has been measured with LCR meter as shown in Figure 4.9.

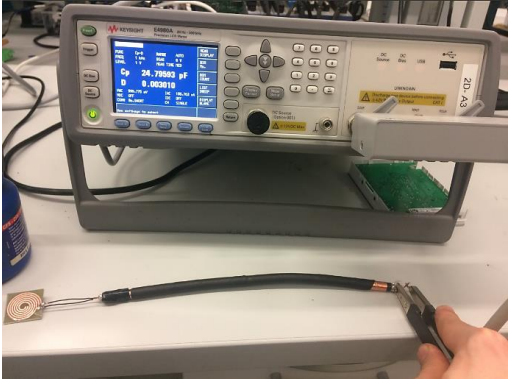


**Figure 4.9 :** Sensor and cable capacitance at 23°C temperature 50% relative humidity 24,79[pF], 12,91[pF] from cable, 11,70[pF] from sensor.

## 5. MEASUREMENTS

The sensor has been inserted to inside of the freezer appliance for testing. One side of the appliance has been drilled and sensor has been fixed inside of the appliance in Figure 5.1. When measuring the sensor without ice, the door of the device was kept closed so that the conditions would be stable. It results about 40,50 [pF] in Figure 5.2. In case of opening the door of appliance during measurements causes the temperature and moisture change inside of the appliance. Warm and moist air covers the cold surfaces. In Figure 5.3 sensor surface and environment are also covered with moisture so the value of the sensor increases. In Figure 5.4 after closing the door, sensor value decreases the again old state by the time about 10 [min].



**Figure 5.1 :** Sensor test without icing in the appliance.

```
t = 456microSeg
C = 0,00 nanoF
C = 41,37 pikof
C = 41371,74 femtoF
C = 41371740,00 attoF
39557,25 ;39557,74 ;
ave;40,50pikof
```

**Figure 5.2 :** 40,50[pF] at -30°C temperature 50% relative humidity 16,18[pF] from circuit, 12,91[pF] from cable 11,41[pF] from sensor.

```
t = 500microSeg
C = 0,00 nanoF
C = 45,45 pikoF
C = 45454,54 femtoF
C = 45454544,00 attoF
43636,36 ;43636,36 ;
ave;44,67pikoF
```

**Figure 5.3 :** Sensor value increases to about 44,67[pF] after door opened.

```

t = 456microSeg
C = 0,00 nanoF
C = 4,14 pikof
C = 41371,80 femtoF
C = 41371800,00 attoF
41557,25 ;41557,25 ;
ave;41,30pikof

```

**Figure 5.4 :** Sensor value about 41,30[pF] after door closed.

In Figure 5.5, when the sensor surface is coated with 1[mm] thick ice that has been prepared before, the sensor value increases to about 51,69[pF] from the about 40,50 [pF] in Figure 5.6. In Figure 5.7 by the time, the iced sensor value decreases to about 46,47[pF]. As a result, when the sensor surface is not covered with ice, the sensor value measured as 11,41[pF] increases to 17,38 [pF] when it is covered with 1[mm] of ice. For the same conditions ANSYS Maxwell results are about 11,32[pF] during without icing sensor and about 13,43[pF] for about 1[mm] ice covering the sensor surface. The difference between values of the sensors which implemented and simulated in case of without icing can be ignored. On the other hand there is a difference about 4[pF] between values of the sensors which implemented and simulated for 1[mm] ice covering. One of the reasons may be that the content of the ice in reality is different from the simulation. Another reason may be that the thickness of the ice can be provided as 1[mm] in simulation, but in fact it is not fully achieved.



**Figure 5.5 :** 1[mm] ice covering to surface of the sensor.

```

t = 568microSeg
C = 0,00 nanoF
C = 51,64 pikof
C = 51636,37 femtoF
C = 51636364,00 attoF
51636,37 ;51636,37 ;
ave;51,69pikof

```

**Figure 5.6 :** Sensor value about 51,69 [pF] after covering with ice as 1[mm] thickness at -30°C temperature 50% relative humidity.



t = 540microSeg	t = 528microSeg	t = 508microSeg
C = 0,00 nanoF	C = 0,00 nanoF	C = 0,00 nanoF
C = 49,09 pikof	C = 48,00 pikof	C = 46,18 pikof
C = 49090,91 femtoF	C = 48000,00 femtoF	C = 46181,82 femtoF
C = 49090908,00 attoF	C = 48000000,00 attoF	C = 46181820,00 attoF
49454,55 ;49454,55 ;	48000,00 ;48000,00 ;	46545,45 ;46545,45 ;
ave;49,47pikof	ave;47,87pikof	ave;46,47pikof

**Figure 5.7 :** Sensor value decreasing to about 46,47[pF] by the time about 10[min].

In case of water drip applying the sensor surface in the appliance as Figure 5.8, the sensor value increases to 49,72[pF] in Figure 5.9. The sensor value decreased to about 48,03[pF] after 10[min] in Figure 5.10.

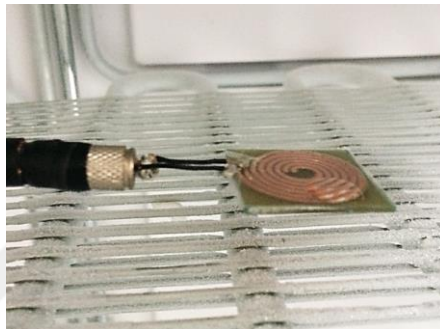


**Figure 5.8 :** Water drip on the sensor surface.

t = 548microSeg
C = 0,00 nanoF
C = 49,72 pikof
C = 49718,74 femtoF
C = 41371874,00 attoF
49718,25 ;49718,74 ;
ave;49,72pikof

**Figure 5.9 :** Sensor value 49,72[pF] in case of water drip at -30°C temperature.

t = 536microSeg	t = 528microSeg
C = 0,00 nanoF	C = 0,00 nanoF
C = 48,63 pikof	C = 47,90 pikof
C = 48630,01 femtoF	C = 47904,19 femtoF
C = 48630010,00 attoF	C = 47904190,00 attoF
48630,01 ;48267,10 ;	48267,10 ;48267,10 ;
ave;48,32pikof	ave;48,03pikof

**Figure 5.10 :** Sensor value decreasing to about 48,03[pF] by the time about 10[min].

In case of water drip to all of the sensor surface in the appliance as Figure 5.11, the sensor value increases to 79,41[pF] in Figure 5.12.



**Figure 5.11** : Water drip to all of the sensor surface.

```
t = 872microseg  
C = 0,00 nanoF  
C = 79,27 pikof  
C = 79272,73 femtoF  
C = 79272728,00 attoF  
79636,36 ;79636,36 ;  
ave;79,41pikof
```

**Figure 5.12** : Sensor value 79,41[pF] in case of water drip to all of the sensor surface at -30°C temperature.

## 6. SENSOR BASED DEFROST ALGORITHM

While the shielding applied to sensor, wire harness and circuit, reduce the effect of parasite, the other environmental factors can affect the measurement result. The SBDA (sensor based defrost algorithm) has been developed in Figure 6.1. for solutions against to unwanted situations.

Situation1: One of these factors which affect the measurement is humidity of the ambient. In case of measuring with the sensor in the compartment of the appliance, when the door of the appliance is opened, warm and moist air enters the compartment. The humidity in the compartment increases with time. Thus, the cold and dry air in the compartment turns into moist and warm air and the sensor is affected by this increase in humidity. The measured value of the sensor increases due to this increasing in humidity during limited period of time. Shortly afterwards, warm and humid air adheres to the cold surfaces which include also sensor surface, and transforms to ice, thereby the sensor value decreases.

Solution1: The checking of the duration after door opening added as a pre-condition for the ice detection. In addition, measurement for 1[ $\text{min}$ ] added for prevent misdetection of the icing due to instant fluctuations.

Situation2: Another factor that affects the measurement is the water dripping on the sensor surface. In case of water dripping to sensor surface, sensor value increases more than the icing situation till water converts to ice due to dielectric constant of the water is higher than ice.

Solution2: A maximum sensor limit as 55[pF] has been added as pre condition. 55[pF] limit was chosen according to the value measured when door was opened and the sensor surface was covered with 1[ $\text{mm}$ ] iced. If the measurement value exceeds the 55[pF] limit, the algorithm continues normal cycle and checks the sensor value after 30[ $\text{min}$ ] again.

Situation3: It is observed that in case of a small amount of water drip on the sensor surface, the value of the sensor does not increase extremely. The sensor value is

about 49,72[pF] for a small amount of water drip to sensor surface. This value is not far from capacitance value which 1[mm] ice covered situation and misdetection is possible.

Solution3: For prevent the misdetection of the water drip as ice, 5[min] delay has been added to algorithm. In this period, small water drip becomes to ice.

As a common pre condition, the ambient temperature checking added for starting the defrost function. The temperature should be equal or smaller than 0°C for ice occurring in the compartment. And, the minimum value in the precondition of the defrost function was selected as 44[pF], with a value of about 46[pF] occurring at 1[mm] of ice thickness.

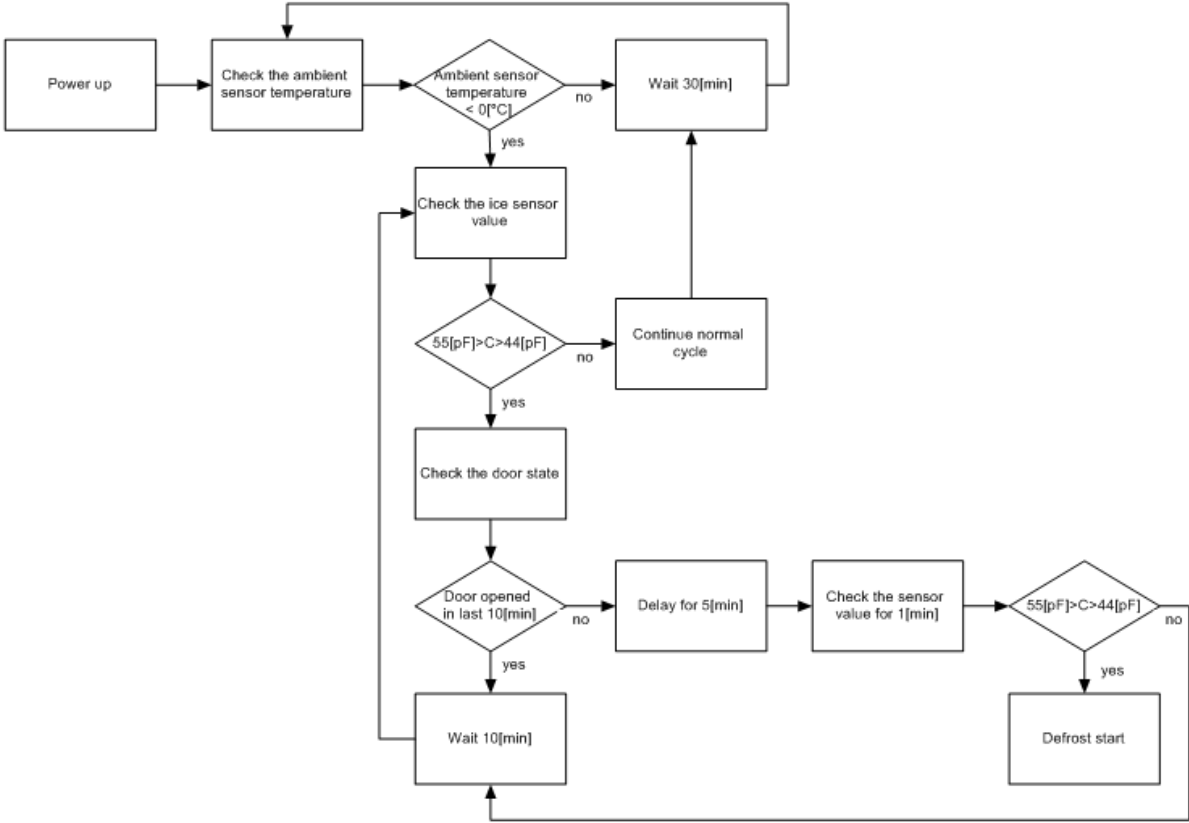


**Figure 6.1 : Sensor Based Defrost Algorithm.**

In the algorithm, the parameter values of sensor and durations have been defined according to test results which have been done during this study. The parameter values can be changed according to appliance type, volume or used sensor number.

## 7. UNCERTAINTY ANALYSIS

In experimental studies, correctness of the measured value is also important as obtained results. The most important factor affecting the accuracy of the measurements is the errors that occurred during the experiments. Error can occur as two different types; experiment set up errors and experimenter error. Experimenter error can be eliminated with experienced and qualified experimenter. But set up error cannot be eliminated easily cause of the it depends on structure of the device and components. Uncertainty analysis is a method developed for the defining the error cause of the set up.

### 7.1 Modeling of the Measurement

The measuring ice thickness can be obtained with a  $y = f(x)$  function. Table 7.1 includes the data from ANSYS Maxwell simulation results for the modeling of the sensor. According to these data, the sensor has been modeled in Figure 7.1 as in equation 7.1.

**Table 7.1** : Ice thickness – sensor capacitance calculations at ANSYS Maxwell.

Capacitance without ice [pF]	Iced capacitance [pF]	Delta [pF]	Ice thickness [mm]
11,327	11,729	0,402	0,10
11,327	12,266	0,939	0,15
11,327	12,504	1,177	0,20
11,327	12,741	1,414	0,25
11,327	13,050	1,723	0,30
11,327	13,105	1,778	0,35
11,327	13,255	1,928	0,40
11,327	13,336	2,009	0,45
11,327	13,475	2,148	0,50
11,327	13,530	2,203	0,55
11,327	13,572	2,245	0,60
11,327	13,643	2,316	0,65
11,327	13,626	2,299	0,70

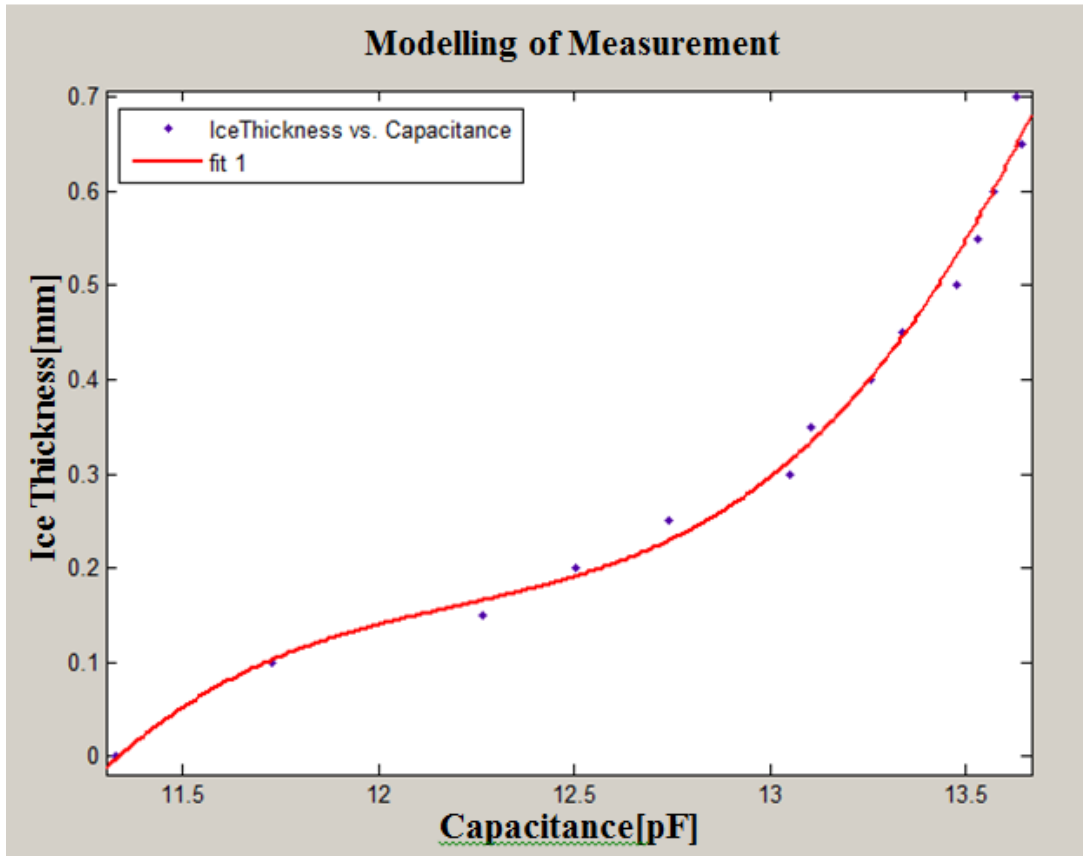


Figure 7.1 : Sensor modeling curve.

$$y = 0,1222x^3 - 4,4716x^2 + 54,64x - 222,8 \quad (7.1)$$

Coefficients with 95% confidence bounds [Url-6].

Definition of the absolute uncertainty has been written as in equation 7.2.

$$W_r = \pm \left[ \left( \frac{\varphi R}{\varphi x_1} w_{x_1} \right)^2 + \left( \frac{\varphi R}{\varphi x_2} w_{x_2} \right)^2 + \dots + \left( \frac{\varphi R}{\varphi x_n} w_{x_n} \right)^2 \right]^{1/2} \quad (7.2)$$

where  $W_r$  is the uncertainty of the measurement circuit,  $n$  is the independent variable,  $R$  is the dimension will be measured,  $x_1, x_2, x_3, \dots, x_n$  are variables which effect to measurement and  $w_{x_1}$  is the error of the independent variables.

The capacitance definition is shown in equation 7.3.

$$C = \frac{T}{1.1 * R_1} \quad (7.3)$$

where  $C$  is the capacitance value which will be measured,  $T$  is the pulse duration of the LM555 timer output and the  $R_1$  is the resistance value which used in the circuit. Real resistance value has been inserted to Software as 10,02[MΩ] in Figure 7.2



**Figure 7.2 :** Resistor value 10,02[MΩ] which used in circuit at 25°C temperature.

The tolerances of the other components which used in circuit are:

Drift with Temperature of resistor: 0,075% (750 ppm) [Url-7].

Accuracy of 16 MHz Arduino Uno oscillator: 0.003% (30ppm) [Url-8].

Drift with Temperature of LM555 timer: 0,005% (50 ppm)

Drift with power supply of LM555 timer:0,1%

The tolerance values has been inserted as below in equation 7.4.

$$W_r = \pm \left[ \left( \frac{0,075}{100} \right)^2 + \left( \frac{0,003}{100} \right)^2 + \left( \frac{0,005}{100} \right)^2 + \left( \frac{0,1}{100} \right)^2 \right]^{\frac{1}{2}} \quad (7.4)$$

Then solution with equaiton 7.5.

$$W_r = \pm [5,6e - 7 + 9e - 10 + 2,5e - 9 + 0,000001]^{\frac{1}{2}} \quad (7.5)$$

The result is  $\pm 0,1\%$  as below equaiton 7.6.

$$W_r \cong \pm 0,1\% \quad (7.6)$$

Combined standad uncertainty written in equation 7.7.

$$u_c(y) = u(x) * \frac{\partial f}{\partial x} \quad (7.7)$$

where  $u_c$  is the combined standard uncertainty and  $u(x)$  is the standard uncertainty. The solution steps have been defined in equation 7.8, equation 7.9, equation 7.10 and equation 7.11 as below.

$$\frac{\partial f}{\partial x} = \frac{\partial y}{\partial x} = 0,3666x^2 - 8,9432x + 54,64 \quad (7.8)$$

$$u_c(y) = u(x) * (0,3666x^2 - 8,9432x + 54,64) \quad (7.9)$$

$$u_c(y) = \frac{0,1x}{100} * (0,3666x^2 - 8,9432x + 54,64) \quad (7.10)$$

$$u_c(y) = 0,0003666x^3 - 0,0089432x^2 + 0,05464x \quad (7.11)$$

The relative uncertainty expressed in equation 7.12 and solved in equation 7.13.

$$\frac{u_c(y)}{y} = \frac{0,0003666x^3 - 0,0089432x^2 + 0,05464x}{y} \quad (7.12)$$

$$\frac{u_c(y)}{y} = \frac{0,0003666x^3 - 0,0089432x^2 + 0,05464x}{0,1222x^3 - 4,4716x^2 + 54,64x - 222,8} \quad (7.13)$$

The results are summarized as below in Table 7.2.



**Table 7.2 : Uncertainty.**

Capacitance [pF]	Thickness [mm]	Combined standard uncertainty	Relative error[%]
11,50	0,04	0,0032	7,59%
11,75	0,10	0,0020	2,08%
12,00	0,13	0,0013	1,02%
12,25	0,16	0,0012	0,77%
12,50	0,18	0,0016	0,89%
12,75	0,23	0,0027	1,18%
13,00	0,29	0,0043	1,48%
13,25	0,40	0,0067	1,68%
13,50	0,55	0,0097	1,77%
13,75	0,76	0,0135	1,77%
14,00	1,04	0,0180	1,73%
14,25	1,41	0,0234	1,66%
14,50	1,87	0,0296	1,58%

## 7.2 Confidence Interval and Standard Deviation

The confidential interval is calculated to find out how much of the values represent the actual values. In large number of measurement series, measurement number  $N > 10$  is assumed to be (Sadikhov, Kangı, and Uğur, 1995). In this study, measurement number  $N = 30$  chosen. Standard devaiton expression shown in equation 7.14 and equation 7.15. The standard deviation calculated from measurements made without connecting the sensor to the circuit Figure 7.3.

$$\sigma = \left[ \frac{1}{N} \sum_{k=1}^N (X_k - \mu)^2 \right]^{\frac{1}{2}} \quad (7.14)$$

$$\sigma = 0,18 \quad (7.15)$$

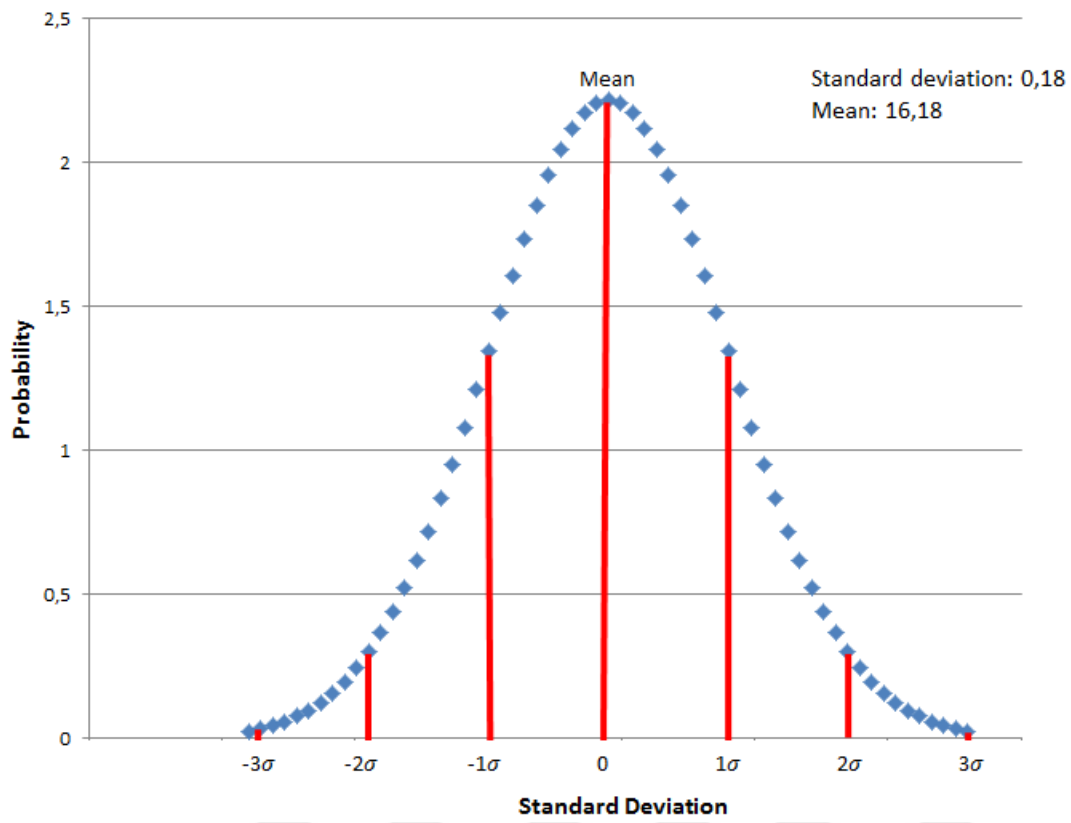


**Figure 7.3 :** Standard deviation graph.

## 8. CONCLUSIONS AND COMMENTS

In this work, a system is designed to detect undesirable icing in refrigerating devices. The designed sensor was tested on the device under real conditions with a signal conditioning circuit. The test results are supported by the simulation results. The sensor, wiring harness and circuit are shielded so that the incoming electrical noise does not affect the measurement result. An algorithm has been proposed to prevent undesirable situations observed during tests from causing false ice detection.

It has been observed that in models made in a simulated environment, the increase in the domain length between the electrodes increases the sensor sensitivity. It has been found that there is a difference of about 3% between the calculated value in the simulation and the capacity value of the implemented sensor. In the case of icing, it is observed that the measured value is 20% higher than the simulation result. The main reason for this difference is thought to be the difference between the value of the dielectric constant in the simulation and the value in the real environment. The reasons for this difference include dust, water-ice content, and so on. The presence of factors is assessed. Screening of the sensor and coating of the domain with insulating material reduced the sensitivity of the sensor. The sensor forming the icing detection system has been tested on conditions close to real icing on the cable group and the circuit cooling device. The reproducibility of the system was found to be high in the tests made. This is an important aspect of the feasibility of the designed structure. With the proposed algorithm, it is tried to prevent possible false icing situations.

When the obtained values are combined with the proposed algorithm, it is considered that a practically applicable system has emerged. In order to ensure the reliability of the system, it is planned to test the system that has been performed for a long time in the cooling devices and the studies in this direction have been started. The difference of 20% observed between measured value and simulation value in the case of ice is considered to be acceptable when our system is considered for practical purposes. However, our efforts to reduce the error and positioning of the sensor in appliance are continuing.



## REFERENCES

- Dialog Semiconductor.** (2015). *IR Windshield Rain Sensor*. (Report No. AN-CM-219). Texas: Dialog Semiconductor.
- Froese, M.** *Cracking the icing problem on turbine blades*. Retrieved March 28, 2017, from <https://www.windpowerengineering.com/business-news-projects/cracking-icing-problem-turbine-blades/>
- Hoover, G. A.** (2017). Aircraft Ice Detectors and Related Technologies for Onground and Inflight Applications. Retrieved <http://www.dtic.mil/dtic/tr/fulltext/u2/a266273.pdf> (Original work published 1993)
- Jiahao, G., Hu, P., Tan, J.** (2016). Analysis of a Segmented Annular Coplanar Capacitive Tilt Sensor with Increased Sensitivity. *sensors*. Retrieved March 11, 2017, from <https://www.ncbi.nlm.nih.gov/pmc/articles/PMC4732166/>
- Krebs, J.** (2015). *Ice Buildup Detection Using TI's Capacitive Sensor Technology*. (Report No. SLLA355). Texas: Texas Instruments Incorporated.
- Martinez, J.** *Build Your Own IR Windshield Rain Sensor*. Retrieved June 28, 2017, from <http://www.electronicdesign.com/automotive/build-your-own-ir-windshield-rain-sensor>
- Aykan, R.M.** (2005). *Aircraft Icing Detection Identification And Reconfigurable Control Based On Kalman Filtering And Neural Network*. (PhD thesis). İstanbul Technical University, GRADUATE SCHOOL OF SCIENCE ENGINEERING AND TECHNOLOGY, ISTANBUL.
- Sadikhov, E., Kangı, R., and Uğur, S.** (1995). *Ölçüm Belirsizliği*. Kocaeli: Ulusal Metroloji Enstitüsü.
- Wang, D.** (2015). *Capacitive Sensing: Ins and Outs of Active Shielding*. (Report No. SNOA926A). Texas: Texas Instruments Incorporated.
- Yichang, W.** (2017). *Capacitive Frost or Ice Detection Reference Design* (Report No. TI Designs: TIDA-01465). Texas: Texas Instruments Incorporated.
- Yu. Ya. Iossel, E. S.** (1969). *The Calculation Of Electrical Capacitance*. Ohio: Foreign Technology Division Air Force Systems Command U. S. Air Force.
- Url-1** <[http://ansoft-maxwell.narod.ru/en/Maxwell\\_v16\\_L01\\_Introduction.pdf](http://ansoft-maxwell.narod.ru/en/Maxwell_v16_L01_Introduction.pdf)>, date retrieved 29.02.2017.
- Url-2** < <https://www.pcbuniverse.com/pcb-tech-tips.php?a=4>>, date retrieved 02.02.2017.

- Url-3** <<https://www.makeitfrom.com/material-properties/Polymethylmethacrylate-PMMA-Acrylic>>, date retrieved 17.04.2017.
- Url-4** <<http://www.ti.com/lit/ds/symlink/lm555.pdf>>, date retrieved 21.12.2016.
- Url-5** <<https://www.arduino.cc/reference/en/language/functions/external-interrupts/attachinterrupt/>>, date retrieved 21.01.2017.
- Url-6** <<https://www.mathworks.com/help/curvefit/confidence-and-prediction-bounds.html>>, date retrieved 11.07.2017.
- Url-7** <<https://www.alliedelec.com/m/d/0ea4dcf244a15ceb022d6f0d143cf695.pdf>>, date retrieved 17.09.2017.
- Url-8** <<https://www.foxonline.com/pdfs/C4ST.pdf>>, date retrieved 21.01.2017.



## **CURRICULUM VITAE**

**Name Surname** : Arda Ađan  
**Place and Date of Birth** : Bakırk6y 19.03.1991  
**E-Mail** : ardaagan@hotmail.com

### **EDUCATION:**

- **B.Sc.** : 2013, Trakya University, Engineering Faculty,  
Mechanical Engineering

### **PROFESSIONAL EXPERIENCE AND REWARDS:**

- 2013-present Research and Development Engineer at BSH Home Appliances  
Development Center Cooling.